Lead-Free Perovskite Single Crystals

Subjects: Crystallography

Contributor: Hanlin Hu

Lead-free perovskites have received remarkable attention because of their nontoxicity, low-cost fabrication, and spectacular properties including controlled bandgap, long diffusion length of charge carrier, large absorption coefficient, and high photoluminescence quantum yield. Compared with the widely investigated polycrystals, single crystals have advantages of lower trap densities, longer diffusion length of carrier, and extended absorption spectrum due to the lack of grain boundaries, which facilitates their potential in different fields including photodetectors, solar cells, X-ray detectors, light-emitting diodes, and so on.

lead-free perovskites | single crystal | high photoluminescence quantum yield | stability

1. Introduction

As a striking material, lead halide perovskites ($APbX_3$) have made unprecedented progress in various fields, such as photodetectors, solar cells, X-ray detectors, light emitting diodes, lasers, transistors, and so on [1][2][3][4][5][6]. The merits of low-cost solution processing and remarkable optoelectronic properties, including tunable bandgap, long carrier lifetime and carrier diffusion length, large absorption coefficient, give lead halide perovskites great potential in the photovoltaic power generation field [7][8][9]. Single-junction perovskite solar cells have realized a certified power conversion efficiency (PCE) of 25.5%, which is comparable to that of silicon-based solar cells [10]. In terms of light emitting, perovskites exhibit a narrow full width at half maximum, high photoluminescence quantum yield (PLQY), and wide color gamut [11]. Meanwhile, photodetectors, transistors, and lasers are also developed rapidly.

However, the severe toxicity and chronic degrading of lead (Pb), the aqueous solubility may cause the contamination of ground water, and the poor stability when exposed to oxygen, heat, moisture and UV light, has retarded the expanded applications of lead halide perovskites [12][13][14]. Although numerous nontoxic elements have been reported as dopants, the residual Pb may still present environmental risk. Hence, the development of low-toxic lead-free perovskites is of great significant to replace the classic $APbX_3$ [15]. Meanwhile, in comparison with polycrystalline perovskites and low-dimension perovskites, perovskite single crystals (PSCs) show excellent optoelectronic properties due to their continuous and unbroken crystal lattices [16], the absence of grain boundaries leads to lower trap densities, longer length for carrier diffusion, and extended absorption spectrum [17][18][19]. Therefore, research of LFPSCs has promoted the enhancement of perovskite materials, and the current high-quality LFPSCs play critical roles in abundant optoelectronic devices.

LFPSCs materials are a series of compounds with a general chemical formula of $A_xB_yX_z$ (x, y, z is up to the structural dimensionality), where A represents an organic or inorganic cation such as MA (CH_3NH_3), FA ($HC(NH_2)_2$,

Cs, Rb, B represents a metal cation (Sn/Sb/Bi/Pd/In/Ti/Pt/Au Cu/Ag), and X represents halide anion (Cl/Br/I). In the metal halide octahedra, B-cation stay at the center of the octahedral, and six X-anions are situated at the six corners, which can grow three-dimensional (3D), two-dimensional (2D), one-dimensional (1D), or zero-dimensional (0D) crystal structures [20][21]. The dimensionality of the perovskite crystal structures mainly depends on the size of the cations and should also fulfill the requirement of Goldschmidt tolerance factor (t),

$$t = \frac{r_A + r_X}{\sqrt{2} \times (r_B + r_X)}$$

where, r_A, r_B, and r_X are the ionic radius of the A-site, B-site, and halide site, respectively. LFPSCs can be classified into four categories based on their crystal structure and the valency of the B cation: (i) divalent metal cation perovskites: ABX_3 (B is +2 oxidation state, B = Sn/Ge/Yb) or layered perovskites $A_2A'_{n-1}B_nX_{3n+1}$; (A′ = long chained organic cations that do not fit in the $[BX_6]^{4-}$ cavity); (ii) trivalent metal cation perovskites: $A_3B_{2\times9}$ (B is +3 oxidation state, B = Sb/Bi); (iii) tetravalent metal cation perovskites: A_2BX_6 (B is +4 oxidation state) (B = Sn/Ge/Pd/Pt); and (iv) double perovskites: $A_2BB'X_6$ (B is +1 while B′ is +3 oxidation states) (B is Au/Ag/ACu; B′ is In/Bi/Sb) [12][22].

2. Various Systems of Pb-Free Single Crystal

In general, lead halide perovskites possess a universal chemical formula of $APbX_3$, where A represents an organic/inorganic cation including Cs^+, methylammonium (MA), formamidinium (FA) or their mixture, and X represents a halide anion which consists of Cl^-, Br^-, I^-, or their mixture. In terms of structure, Pb^{2+} cations are separated by six neighbor X-site anions to bulid Pb-X octahedrons, which corner-share with each other to constitute the main frame and A^+ intercalates the voids [23]. The replacement of Pb^{2+} with lead-free ions results in both the deformation in nanoscale structure and the conversion of properties because of the differences in chemical valence and ion size [24]. Therefore, LFPSCs exhibit plenty of novelty and diversity.

2.1. Sn Based Halide Perovskites

Attributed to the same valence and similar properties with Pb^{2+}, Sn^{2+} is seen as a crucial candidate to form lead-free perovskites without the sacrifice of the excellent performance. The first Sn-based halide perovskite single crystals were synthesized in 1974 for $CsSnX_3$ [25]. In 2012, Chung et al. prepared $CsSnI_3$single crystals using a modified vertical Bridgman technique with refined crystal structure and optical properties [26]. Due to the crystal structure transformation from α-phase to γ-phase during the preparation of $CsSnI_3$, the crystal configuration of $CsSnI_3$ is not cubic symmetry, but the stable γ-phase $CsSnI_3$ SC (direct bandgap =1.3 eV) at room temperature, showing a p-type semiconductor behavior with a carrier concentration and a hole mobility of ≈10^{17} cm^{-3} and ≈585 cm^2 V^{-1} s^{-1}, respectively. A similar result has been reported in $FASnI_3$ perovskite single crystals by Kahmann et al. [27].

2.2. Bi/Sb Based Halide Perovskites

Trivalent ions such as Bi^{3+} and Sb^{3+} are also considered as the alternatives for LFPSCs. Generally, B^{3+} can form a perovskite-like derivate—$A_3B_2X_9$, with 0D or 2D crystal structures. The initial exploration started by Lehner and co-workers in 2015 [28]. They found A and X atoms are closest-packed while B atoms occupy 2/3 voids of the octahedral X_6, and the crystal structures of $A_3B_2X_9$ can be classified into two typical types: cubic close-packing and hexagonal close-packing of A and X atoms. Changes of A cation lead to significant differences in structural configurations and properties. To be specific, $Cs_3Bi_2I_9$ single crystal tends to form a 0D configuration attributed to the isolated $[Bi_2X_9]$ structures, which is resulted from the face-sharing $[BiX_6]$ octahedron. By contrast, $K_3Bi_2I_9$ and $Rb_3Bi_2I_9$ tend to generate layer-like 2D structures. Another popular trivalent ion is Sb^{3+}. McCall and co-workers synthesized $Cs_3Bi_2I_9$ and $Rb_3Bi_2I_9$ SCs by the Bridgman method and characterized their crystal structures by SCs X-ray diffraction, showing $[SbI_6]$ octahedrons and isolating alkali ions for both of them. For optoelectronic properties, they display broad PL emission from 1.75 to 2.05 eV with two peaks located at 1.96 and 1.92 eV, respectively [29]. Besides that, these scholars have made a further investigation on other derivatives, after optimizing the synthesis of single crystal, they implemented the photo-response to observe visible laser emission of $Cs_3Bi_2I_9$ for the first time. All SCs showed ambipolar response to Am α-particles irradiation with spectra for both electron and hole collection configurations, and it is worth noting that $Cs_3Bi_2I_9$ and $Cs_3Sb_2I_9$ showed a superb potential for radiation detection [30].

2.3. Other Metals Based Perovskites

Researchers have also developed some other metal-based PSCs, such as from indium, copper. In the work of Zhou et al., they employed a slow-cooling crystal growth approach by blending CsBr and $InBr_3$ in HBr at 130 °C for 0.5 h [31]. After cooling down to room temperature, 0D $Cs_2InBr_5{:}H_2O$ was obtained with a size of around 2 mm. It shows a 0D orthorhombic crystal structure where the $[InBr_5O]_4^-$ octahedrons were separated by two Cs^+-cations. It also displays a bright red luminescence peak at 695 nm with a PLQY of 33% under excitation of 365 nm. Other 0D $(C_4H_{14}N_2)_2InBr_{10}$ PSCs were synthesized within several minutes by adding $InBr_3$ solution (dissolved in HBr acid) into a mixture of diethylamine and HBr at 0 °C [32]. The In-Br polyhedrons were separated by the $(C_4H_{14}N_2)^{2+}$-cations to produce a 0-D perovskite-like structure. It exhibits an abrupt absorption from 350 to 600 nm and a broad band emission from 500 nm and near-infrared region attributes to the structural distortion of $[InBr_6]^{3-}$ octahedral units leading to the formation of self-trapped exciton (STE) states, confirmed also by computational study.

2.4. Halide Double Perovskites

Apart from single B-site ions-based lead-free perovskite, double perovskites with a formula of $A_2B'B''X_6$ have been investigated due to their excellent performance [33][34][35]. Pan et al. used a solution-process approach to obtain double perovskite $Cs_2AgBiBr_6$ single crystals, where centers of the metal bromide octahedron are occupied by alternate Bi^{3+} and Ag^+. They proposed the presence of cations disorder during the growth process, resulting in the destroyed symmetry of double perovskite. Thermal annealing and surface treatment could eliminate these defects and improve the crystal resistivity effectively [36]. After that, numerous researchers have accomplished research on $Cs_2AgBiBr_6$ [37][38][39][40], in the work of Zhang et al., the resistivity of the $Cs_2AgBiBr_6$ was larger than 10^{10} Ω cm, the Fermi level was estimated to be 0.788 eV above the valence band and the two near bandgap energies were

1.917 eV and 2.054 eV, respectively [37]. Keshavarz and co-workers employed alkali substitution to tune the structures and properties of $Cs_2AgBiBr_6$ double perovskites. The fundamental lifetime of carrier recombination at room temperature attained a three-fold increase with the band gap remaining unchanged [40]. Furthermore, Yin et al. synthesized $Cs_2AgIn_xFe_{1-x}Cl_6$ ($0 < x < 1$) perovskite SCs employing a simple hydrothermal method, which exhibited a broadband absorbance from 450 to 800 nm and a huge enhancement of PLQY [41].

3. Applications

LFPSCs possess numerous fascinating optoelectronic properties in practical applications, as shown in **Figure 1**. Even if there is still a certain gap between lead-free and lead-based PSCs, several applications of LFPSCs have attracted attention recently. Herein, the reported achievements of applications using LFPSCs, such as photodetectors, solar cells, X-ray detectors, light emitting diodes, and other applications (**Figure 2**).

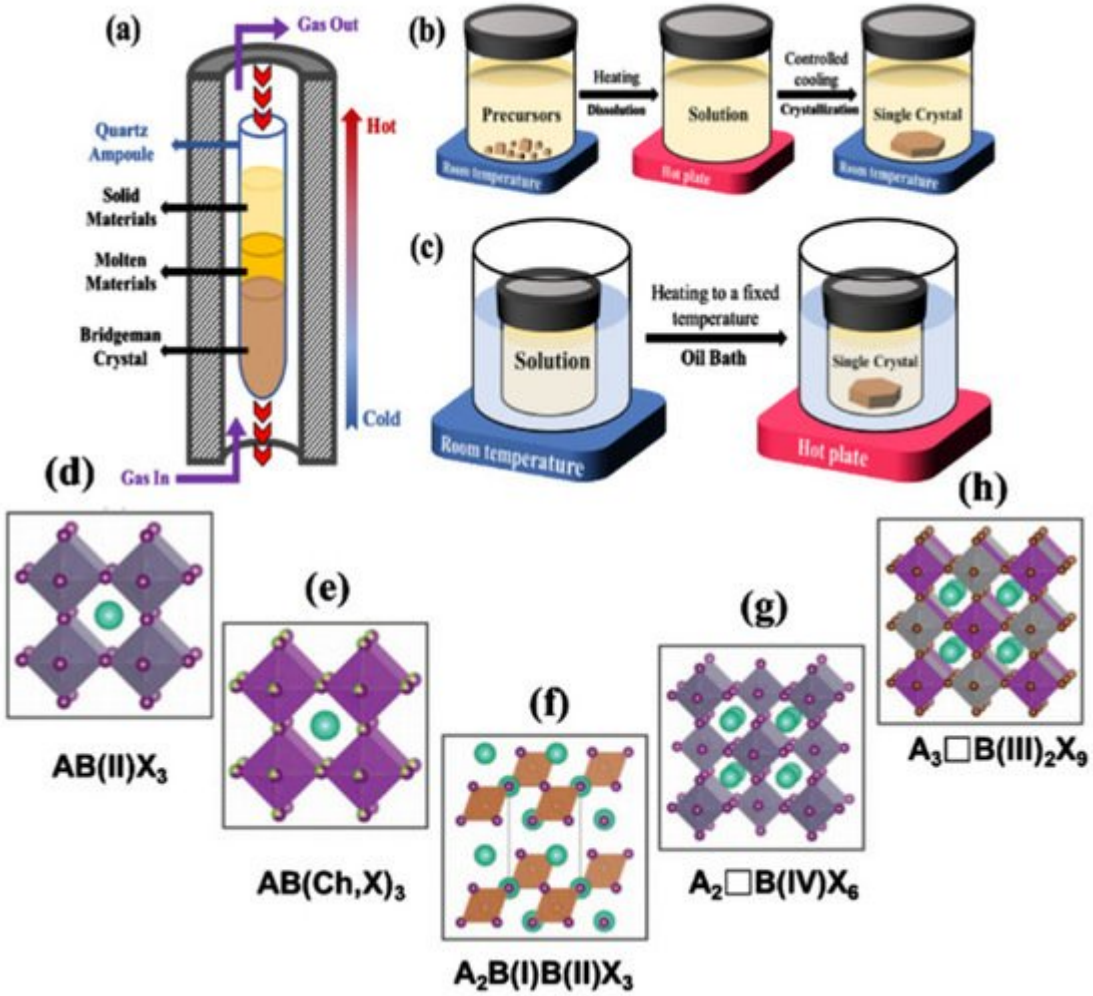

Figure 1. Schematic diagrams of synthesis methods of LFPSCs. (**a**) Bridgeman method. (**b**) Cooling-induced crystallization method. (**c**) Inverse temperature crystallization. (**d**–**h**) Typical crystal structures of LFPSCs. Reprinted (adapted) with permission from Reference 12. Copyright 2020 Elsevier Ltd. Reprinted (adapted) with permission from Reference [22]. Copyright 2021 American Chemical Society.

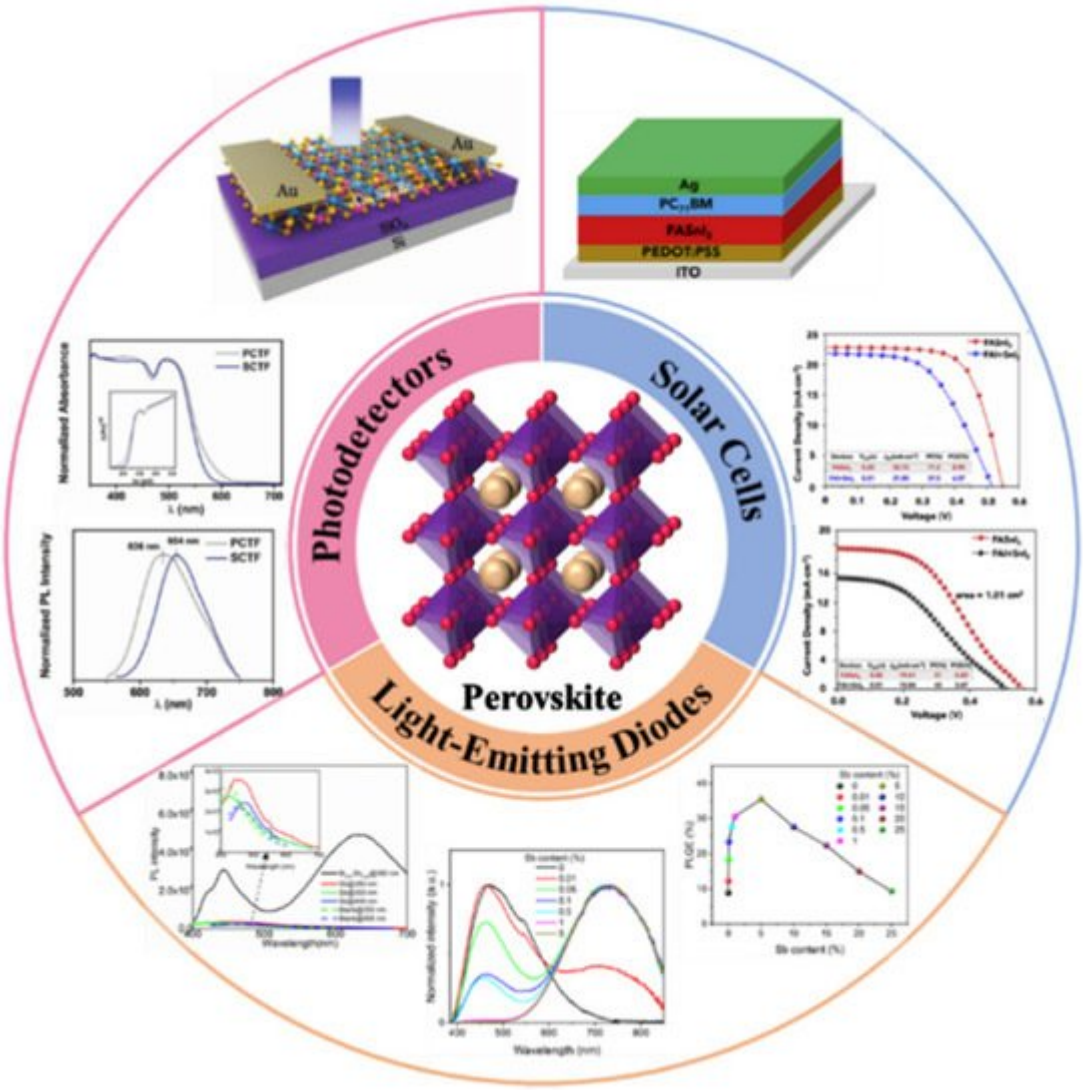

Figure 2. Illustration of various remarkable properties of LFPSCs in practical applications, including photodetectors, X-ray detectors, and light-emitting diodes. Reprinted (adapted) with permission from Reference [24]. Copyright 2021 WILEY-VCH Verlag GmbH & Co. KGaA, Weinheim.

3.1. Photodetectors

Photodetectors capture optical signals and convert them into electrical signals instantaneously, which have been widely employed in abundant fields. The key factors of excellent photodetectors can be summarized as fast responding speed, high photocurrent intensity, and low detectivity.

Liu et al. reported a blue light photodetector with a structure of $Si/SiO_2/Cs_3Sb_2Br_9/Au$, the device possessed low dark current (2.4×10^{-12} A) and impressive photocurrent (3.1×10^{-8} A) at a bias of 6 V under dark condition and illuminated by 480 nm light, the response and recovery time was 0.2 ms and 3 ms respectively [42]. Compared with other lead-free perovskite-based photodetectors, Zheng et al. fabricated a nanoflake photodetector demonstrating a response speed of 24/48 ms [43].

3.2. Solar Cells

He et al. fabricated the device using synthesized $FASnI_3$ single crystals as precursors, which possessed high purity, low defect density, and excellent stability in the air [44]. The authors demonstrated that re-dissolved single crystals forming solution effectively prevents the oxidation of Sn^{2+} by reducing impurities and moisture. The single crystal precursors-based films showed smooth morphology and exhibited larger and more uniform grains than conventional films. The PCE of device was 8.9% and 5.5% for spin-coated solar cells and large-scale printed cells, respectively. In addition, $FASnI_3$ single crystal precursors-based devices retained a higher percentage of initial PCE than conventional devices. The precise controlling of crystallization to obtain near-single-crystalline film is also a viable approach to achieve higher performance.

3.3. X-ray Detectors

X-ray detection plays an important role for scientific study, medical diagnosis, and industrial inspection [12][45]. LFPSCs can be good candidates for X-ray detection because of some unique properties including large X-ray attenuation coefficients; a suitable bandgap (1.5 to 5.0 eV); highly crystalline with lower trap density; large bulk resistivity with less ion migration; high sensitivity and stability; and low toxicity [46][47]. The detection of X-ray has been of great importance due to the wide applications of X-ray in various fields, and some relevant works are summarized in **Table 1** on this topic.

Table 1. X-ray detection parameters of LFPSCs based devices.

LEPSCs	μτ Product (cm^2V^{-1})	Sensitivity ($\mu C \cdot Gyair^{-1} \cdot cm^{-2}$)	Detection limit ($nGyairs^{-1}$)	Ref.
$Cs_2AgBiBr_6$	6.3×10^{-3}	316.8	59.7	[36]
$Cs_2AgBiBr_6$	5.95×10^{-3}	1974	226.2	[48]
$MA_3Bi_2I_9$	NA	1947	83	[49]
$Cs_3Bi_2I_9$	7.97×10^{-4}	1652.3	130	[50]
$(BA)_2CsAgBiBr_7$	1.21×10^{-3}	4.2	NA	[51]
$(H_2MDAP)BiI_5$	NA	1.0	NA	[52]

3.4. Light-Emitting Diodes

Another important optoelectronic application of perovskites is light-emitting diodes (LED) because of their PLQY, tunable band gap, and facile solution preparation. For LFPSCs, low-dimensional halide perovskites have attracted remarkable attention for their spectacular photoluminescence properties and chemical stability, also, the doping strategies have been widely adopted to enable or balance multiple emission centers [53][54][55]. In 2019, a $(C_8NH_{12})_4Bi_{0.57}Sb_{0.43}Br_7 \cdot H_2O$ SCs was synthesized and showed ultra-broadband emission spectrum between 400 and 850 nm, with a PLQY value increased from 0.7% ($(C_8NH_{12})_4BiBr_7 \cdot H_2O$) to 4.5% [53].

3.5. Humidity Sensor and Field-Effect Transistors

Besides the above-mentioned applications, Pb-free PSCs were also employed into other promising applications. Zhou et al. prepared a Pb-free 0D $Cs_2InBr_5 \cdot H_2O$ PSC with a broad red luminescence centered at 695 nm and a high PLQY up to 33%, resulting from the deformations of charge carriers via STE states [31]. It exhibits different emission in a moisture-containing condition with good structural- and photo-stability. A PL humidity sensor was fabricated based on switchable dual emission corresponding to the hydrated and dehydrated states, showing good recyclability and fast response time. This pioneering work establishes a foothold for the utilization of Pb-free perovskite in humidity detection and also demonstrates the advantages of exploring novel applications for these Pb-free perovskite materials.

4. Challenges and Prospects

The current challenges and prospects of LFPSCs are summarized as follows:

(1) The performance of LFPSCs extremely depends on the synthesis methods, hence the exploration of controllable and reliable synthesis to yield stable and high-quality single crystals is necessary to be focused on, with economic and environmental factors under consideration. Moreover, the precise control of thickness and size could be effective approaches to enhance the performance of different devices.

(2) The doping strategies, employed to improve properties, are universal in the research of LFPSCs, but the specific enhancement mechanism has not been thoroughly studied. The intensive study of dopants contributes to obtaining tunable and enhanced single crystals. Most LFPSCs possess wide bandgap which exhibited a narrow range absorption of the solar spectrum. It is important to design more materials with favorable bandgaps and study the structure-property correlation systematically by tuning their bandgaps through halide exchange.

(3) The reproducibility of LFPSCs based devices remains a huge challenge. Almost all the reported devices are fabricated based on lab-scale. They demonstrated batch-to-batch variations, and most of their results cannot be reproduced. The properties of the synthesized materials highly depended on the operator and condition for processing, storage.

(4) The large thickness of LFPSC along the direction of carrier transportation may lead to low current density, while the fabricating technologies of devices also suppress the PCE of solar cells.

(5) Stability of LEFPSs is another important issue. Therefore, huge efforts should be devoted to improve crystal stability as well as maintain their excellent photophysical and chemical properties.

References

1. Zhao, Q.; Hazarika, A.; Chen, X.; Harvey, S.P.; Larson, B.W.; Teeter, G.R.; Liu, J.; Song, T.; Xiao, C.; Shaw, L.; et al. High efficiency perovskite quantum dot solar cells with charge separating heterostructure. Nat. Commun. 2019, 10, 2842.
2. Wei, Y.; Cheng, Z.; Lin, J. An overview on enhancing the stability of lead halide perovskite quantum dots and their applications in phosphor-converted LEDs. Chem. Soc. Rev. 2019, 48, 310–350.
3. Wang, H.; Kim, D.H. Perovskite-based photodetectors: Materials and devices. Chem. Soc. Rev. 2017, 46, 5204–5236.
4. Jeong, J.; Kim, M.; Seo, J.; Lu, H.; Ahlawat, P.; Mishra, A.; Yang, Y.; Hope, M.A.; Eickemeyer, F.T.; Kim, M.; et al. Pseudo-halide anion engineering for alpha-FAPbI3 perovskite solar cells. Nature 2021, 592, 381–385.
5. Dou, L.; Yang, Y.M.; You, J.; Hong, Z.; Chang, W.H.; Li, G.; Yang, Y. Solution-processed hybrid perovskite photodetectors with high detectivity. Nat. Commun. 2014, 5, 5404.
6. Yin, W.-J.; Shi, T.; Yan, Y. Unusual defect physics in CH3NH3PbI3 perovskite solar cell absorber. Appl. Phys. Lett. 2014, 104, 063903.
7. Wang, Q.; Wang, X.; Yang, Z.; Zhou, N.; Deng, Y.; Zhao, J.; Xiao, X.; Rudd, P.; Moran, A.; Yan, Y.; et al. Efficient sky-blue perovskite light-emitting diodes via photoluminescence enhancement. Nat. Commun. 2019, 10, 5633.
8. Shamsi, J.; Urban, A.S.; Imran, M.; De Trizio, L.; Manna, L. Metal Halide Perovskite Nanocrystals: Synthesis, Post-Synthesis Modifications, and Their Optical Properties. Chem. Rev. 2019, 119, 3296–3348.
9. Lin, K.; Xing, J.; Quan, L.N.; de Arquer, F.P.G.; Gong, X.; Lu, J.; Xie, L.; Zhao, W.; Zhang, D.; Yan, C. Perovskite light-emitting diodes with external quantum efficiency exceeding 20 per cent. Nature 2018, 562, 245–248.
10. Min, H.; Lee, D.Y.; Kim, J.; Kim, G.; Lee, K.S.; Kim, J.; Paik, M.J.; Kim, Y.K.; Kim, K.S.; Kim, M.G.; et al. Perovskite solar cells with atomically coherent interlayers on SnO2 electrodes. Nature 2021, 598, 444–450.
11. Luo, J.; Hu, M.; Niu, G.; Tang, J. Lead-free halide perovskites and perovskite variants as phosphors toward light-emitting applications. ACS Appl. Mater. Interfaces 2019, 11, 31575–31584.
12. Bhaumik, S.; Ray, S.; Batabyal, S.K. Recent advances of lead-free metal halide perovskite single crystals and nanocrystals: Synthesis, crystal structure, optical properties, and their diverse applications. Mater. Today Chem. 2020, 18, 100363.
13. Jiang, H.; Kloc, C. Single-crystal growth of organic semiconductors. MRS Bull. 2013, 38, 28–33.

14. Deng, Y.; Xiao, Z.; Huang, J. Light-Induced Self-Poling Effect on Organometal Trihalide Perovskite Solar Cells for Increased Device Efficiency and Stability. Adv. Energy Mater. 2015, 5, 1500721.
15. Akkerman, Q.A.; Raino, G.; Kovalenko, M.V.; Manna, L. Genesis, challenges and opportunities for colloidal lead halide perovskite nanocrystals. Nat. Mater. 2018, 17, 394–405.
16. Song, Y.; Bi, W.; Wang, A.; Liu, X.; Kang, Y.; Dong, Q. Efficient lateral-structure perovskite single crystal solar cells with high operational stability. Nat. Commun. 2020, 11, 274.
17. Jing, L.; Cheng, X.; Yuan, Y.; Du, S.; Ding, J.; Sun, H.; Zhan, X.; Zhou, T. Design Growth of Triangular Pyramid MAPbBr3 Single Crystal and Its Photoelectric Anisotropy between (100) and (111) Facets. J. Phys. Chem. C 2019, 123, 10826–10830.
18. Yang, C.; El-Demellawi, J.K.; Yin, J.; Velusamy, D.B.; Emwas, A.-H.M.; El-Zohry, A.M.; Gereige, I.; AlSaggaf, A.; Bakr, O.M.; Alshareef, H.N.; et al. MAPbI3 Single Crystals Free from Hole-Trapping Centers for Enhanced Photodetectivity. ACS Energy Lett. 2019, 4, 2579–2584.
19. Chen, Y.; He, M.; Peng, J.; Sun, Y.; Liang, Z. Structure and Growth Control of Organic-Inorganic Halide Perovskites for Optoelectronics: From Polycrystalline Films to Single Crystals. Adv. Sci. 2016, 3, 1500392.
20. Chakraborty, S.; Xie, W.; Mathews, N.; Sherburne, M.; Ahuja, R.; Asta, M.; Mhaisalkar, S.G. Rational Design: A High-Throughput Computational Screening and Experimental Validation Methodology for Lead-Free and Emergent Hybrid Perovskites. ACS Energy Lett. 2017, 2, 837–845.
21. Giustino, F.; Snaith, H.J. Toward Lead-Free Perovskite Solar Cells. ACS Energy Lett. 2016, 1, 1233–1240.
22. Tailor, N.K.; Kar, S.; Mishra, P.; These, A.; Kupfer, C.; Hu, H.; Awais, M.; Saidaminov, M.; Dar, M.I.; Brabec, C.; et al. Advances in Lead-Free Perovskite Single Crystals: Fundamentals and Applications. ACS Mater. Lett. 2021, 3, 1025–1080.
23. Akkerman, Q.A.; Manna, L. What defines a halide perovskite? ACS Energy Lett. 2020, 5, 604–610.
24. Zhao, S.; Cai, W.; Wang, H.; Zang, Z.; Chen, J. All-Inorganic Lead-Free Perovskite(-Like) Single Crystals: Synthesis, Properties, and Applications. Small Methods 2021, 5, 2001308.
25. Scaife, D.E.; Weller, P.F.; Fisher, W.G. Crystal preparation and properties of cesium tin (II) trihalides. J. Solid State Chem. 1974, 9, 308–314.
26. Chung, I.; Song, J.-H.; Im, J.; Androulakis, J.; Malliakas, C.D.; Li, H.; Freeman, A.J.; Kenney, J.T.; Kanatzidis, M.G. CsSnI3: Semiconductor or metal? High electrical conductivity and strong near-infrared photoluminescence from a single material. High hole mobility and phase-transitions. J. Am. Chem. Soc. 2012, 134, 8579–8587.

27. Kahmann, S.; Nazarenko, O.; Shao, S.; Hordiichuk, O.; Kepenekian, M.; Even, J.; Kovalenko, M.V.; Blake, G.R.; Loi, M.A. Negative Thermal Quenching in FASnI3 Perovskite Single Crystals and Thin Films. ACS Energy Lett. 2020, 5, 2512–2519.
28. Lehner, A.J.; Fabini, D.H.; Evans, H.A.; Hébert, C.-A.; Smock, S.R.; Hu, J.; Wang, H.; Zwanziger, J.W.; Chabinyc, M.L.; Seshadri, R. Crystal and Electronic Structures of Complex Bismuth Iodides A3Bi2I9 (A = K, Rb, Cs) Related to Perovskite: Aiding the Rational Design of Photovoltaics. Chem. Mater. 2015, 27, 7137–7148.
29. McCall, K.M.; Stoumpos, C.C.; Kostina, S.S.; Kanatzidis, M.G.; Wessels, B.W. Strong Electron–Phonon Coupling and Self-Trapped Excitons in the Defect Halide Perovskites A3M2I9 (A = Cs, Rb; M = Bi, Sb). Chem. Mater. 2017, 29, 4129–4145.
30. McCall, K.M.; Liu, Z.; Trimarchi, G.; Stoumpos, C.C.; Lin, W.; He, Y.; Hadar, I.; Kanatzidis, M.G.; Wessels, B.W. α-Particle Detection and Charge Transport Characteristics in the A3M2I9Defect Perovskites (A = Cs, Rb; M = Bi, Sb). ACS Photonics 2018, 5, 3748–3762.
31. Zhou, L.; Liao, J.; Huang, Z.; Wei, J.; Wang, X.; Li, W.; Chen, H.; Kuang, D.; Su, C. A Highly Red-Emissive Lead-Free Indium-Based Perovskite Single Crystal for Sensitive Water Detection. Angew. Chem. Int. Ed. 2019, 58, 5277–5281.
32. Zhou, L.; Liao, J.; Huang, Z.; Wei, J.; Wang, X.; Chen, H.; Kuang, D. Intrinsic Self-Trapped Emission in 0D Lead-Free (C4H14N2)2In2Br10 Single Crystal. Angew. Chem. Int. Ed. 2019, 58, 15435–15440.
33. Slavney, A.H.; Hu, T.; Lindenberg, A.M.; Karunadasa, H.I. A Bismuth-Halide Double Perovskite with Long Carrier Recombination Lifetime for Photovoltaic Applications. J. Am. Chem. Soc. 2016, 138, 2138–2141.
34. Wu, C.; Zhang, Q.; Liu, Y.; Luo, W.; Guo, X.; Huang, Z.; Ting, H.; Sun, W.; Zhong, X.; Wei, S. The dawn of lead-free perovskite solar cell: Highly stable double perovskite Cs2AgBiBr6 film. Adv. Sci. 2018, 5, 1700759.
35. Ning, W.; Gao, F. Structural and functional diversity in lead-free halide perovskite materials. Adv. Mater. 2019, 31, 1900326.
36. Pan, W.; Wu, H.; Luo, J.; Deng, Z.; Ge, C.; Chen, C.; Jiang, X.; Yin, W.-J.; Niu, G.; Zhu, L.; et al. Cs2AgBiBr6 single-crystal X-ray detectors with a low detection limit. Nat. Photonics 2017, 11, 726–732.
37. Zhang, Z.; Yang, G.; Zhou, C.; Chung, C.-C.; Hany, I. Optical and electrical properties of all-inorganic Cs2AgBiBr6 double perovskite single crystals. RSC Adv. 2019, 9, 23459–23464.
38. Steele, J.A.; Pan, W.; Martin, C.; Keshavarz, M.; Debroye, E.; Yuan, H.; Banerjee, S.; Fron, E.; Jonckheere, D.; Kim, C.W.; et al. Photophysical Pathways in Highly Sensitive Cs2 AgBiBr6 Double-Perovskite Single-Crystal X-Ray Detectors. Adv. Mater. 2018, 30, e1804450.

39. Zhang, Z.; Chung, C.-C.; Huang, Z.; Vetter, E.; Seyitliyev, D.; Sun, D.; Gundogdu, K.; Castellano, F.N.; Danilov, E.O.; Yang, G. Towards radiation detection using Cs2AgBiBr6 double perovskite single crystals. Mater. Lett. 2020, 269, 127667.
40. Keshavarz, M.; Debroye, E.; Ottesen, M.; Martin, C.; Zhang, H.; Fron, E.; Küchler, R.; Steele, J.A.; Bremholm, M.; Van de Vondel, J. Tuning the Structural and Optoelectronic Properties of Cs2AgBiBr6 Double-Perovskite Single Crystals through Alkali-Metal Substitution. Adv. Mater. 2020, 32, 2001878.
41. Yin, H.; Xian, Y.; Zhang, Y.; Chen, W.; Wen, X.; Rahman, N.U.; Long, Y.; Jia, B.; Fan, J.; Li, W. An Emerging Lead-Free Double-Perovskite Cs2AgFeCl6: In Single Crystal. Adv. Funct. Mater. 2020, 30, 2002225.
42. Liu, P.; Liu, Y.; Zhang, S.; Li, J.; Wang, C.; Zhao, C.; Nie, P.; Dong, Y.; Zhang, X.; Zhao, S.; et al. Lead-Free Cs3Sb2Br9 Single Crystals for High Performance Narrowband Photodetector. Adv. Opt. Mater. 2020, 8, 2001072.
43. Zheng, Z.; Hu, Q.; Zhou, H.; Luo, P.; Nie, A.; Zhu, H.; Gan, L.; Zhuge, F.; Ma, Y.; Song, H.; et al. Submillimeter and lead-free Cs3Sb2Br9 perovskite nanoflakes: Inverse temperature crystallization growth and application for ultrasensitive photodetectors. Nanoscale Horiz. 2019, 4, 1372–1379.
44. He, L.; Gu, H.; Liu, X.; Li, P.; Dang, Y.; Liang, C.; Ono, L.K.; Qi, Y.; Tao, X. Efficient anti-solvent-free spin-coated and printed Sn-perovskite solar cells with crystal-based precursor solutions. Matter 2020, 2, 167–180.
45. Li, Y.; Yang, T.; Xu, Z.; Liu, X.; Huang, X.; Han, S.; Liu, Y.; Li, M.; Luo, J.; Sun, Z. Dimensional Reduction of Cs2AgBiBr6: A 2D Hybrid Double Perovskite with Strong Polarization Sensitivity. Angew. Chem. Int. Ed. 2020, 59, 3429–3433.
46. Shi, C.; Ye, L.; Gong, Z.-X.; Ma, J.-J.; Wang, Q.-W.; Jiang, J.-Y.; Hua, M.-M.; Wang, C.-F.; Yu, H.; Zhang, Y.; et al. Two-Dimensional Organic–Inorganic Hybrid Rare-Earth Double Perovskite Ferroelectrics. J. Am. Chem. Soc. 2020, 142, 545–551.
47. Guo, W.; Liu, X.; Han, S.; Liu, Y.; Xu, Z.; Hong, M.; Luo, J.; Sun, Z. Room-Temperature Ferroelectric Material Composed of a Two-Dimensional Metal Halide Double Perovskite for X-ray Detection. Angew. Chem. Int. Ed. 2020, 59, 13879–13884.
48. Yin, L.; Wu, H.; Pan, W.; Yang, B.; Li, P.; Luo, J.; Niu, G.; Tang, J. Controlled cooling for synthesis of Cs2AgBiBr6 single crystals and its application for X-ray detection. Adv. Opt. Mater. 2019, 7, 1900491.
49. Liu, Y.; Xu, Z.; Yang, Z.; Zhang, Y.; Cui, J.; He, Y.; Ye, H.; Zhao, K.; Sun, H.; Lu, R. Inch-size 0D-structured lead-free perovskite single crystals for highly sensitive stable X-ray imaging. Matter 2020, 3, 180–196.

50. Zhang, Y.; Liu, Y.; Xu, Z.; Ye, H.; Yang, Z.; You, J.; Liu, M.; He, Y.; Kanatzidis, M.G.; Liu, S. Nucleation-controlled growth of superior lead-free perovskite Cs3Bi2I9 single-crystals for high-performance X-ray detection. Nat. Commun. 2020, 11, 2304.
51. Xu, Z.; Liu, X.; Li, Y.; Liu, X.; Yang, T.; Ji, C.; Han, S.; Xu, Y.; Luo, J.; Sun, Z. Exploring Lead-Free Hybrid Double Perovskite Crystals of (BA) 2CsAgBiBr7 with Large Mobility-Lifetime Product toward X-Ray Detection. Angew. Chem. Int. Ed. 2019, 58, 15757–15761.
52. Tao, K.; Li, Y.; Ji, C.; Liu, X.; Wu, Z.; Han, S.; Sun, Z.; Luo, J. A Lead-Free Hybrid Iodide with Quantitative Response to X-ray Radiation. Chem. Mater. 2019, 31, 5927–5932.
53. Zhang, R.; Mao, X.; Yang, Y.; Yang, S.; Zhao, W.; Wumaier, T.; Wei, D.; Deng, W.; Han, K. Air-Stable, Lead-Free Zero-Dimensional Mixed Bismuth-Antimony Perovskite Single Crystals with Ultra-broadband Emission. Angew. Chem. Int. Ed. Engl. 2019, 58, 2725–2729.
54. Li, Z.; Song, G.; Li, Y.; Wang, L.; Zhou, T.; Lin, Z.; Xie, R.J. Realizing Tunable White Light Emission in Lead-Free Indium(III) Bromine Hybrid Single Crystals through Antimony(III) Cation Doping. J. Phys. Chem. Lett. 2020, 11, 10164–10172.
55. Jing, Y.; Liu, Y.; Jiang, X.; Molokeev, M.S.; Lin, Z.; Xia, Z. Sb3+ Dopant and Halogen Substitution Triggered Highly Efficient and Tunable Emission in Lead-Free Metal Halide Single Crystals. Chem. Mater. 2020, 32, 5327–5334.